RSC Advances

PAPER

Hybrid nanocomposite films of polyvinyl alcohol and ZnO as interactive gas barrier layers for electronics device passivation†

Satyajit Gupta,[ab] **S. Sindhu,**[b] **K. Arul Varman,**[a] **Praveen C. Ramamurthy***[ab] **and Giridhar Madras**[b]

The development of low cost, easy processable, barrier encapsulant materials is of critical importance for the rapid commercialization of organic/electronic devices. In this study, flexible and thermally stable composites were prepared by simple solution processing using polyvinyl alcohol as the base polymer matrix and reactive zinc oxide nanoparticles as the dispersed phase. These materials were characterized for their applications as barrier materials for moisture and oxygen sensitive organic devices. Various studies such as thermal analysis, mechanical analysis, surface analysis and permeability studies were used to characterize the composite films for their possible use as a passivation material. The material was used to encapsulate Schottky structured devices, and the performance of these encapsulated devices under accelerated weathering was studied.

Introduction

Gas barrier materials/thin films have applications in various fields such as organic electronic device encapsulation and food/pharmaceutical packaging industries. In the case of organic devices (OLED, OPVD and OFET) and dye sensitized solar cells, the instability of the devices is primarily caused by moisture and oxygen.[1–3] Devices can be protected by conformally and hermetically enclosing them with a suitable lightweight gas barrier material. The application of the barrier films in a particular field depends on the material's barrier properties to gases/vapors. Polymer nanocomposite materials and hybrid materials can be used as a promising barrier material for electronic devices and also can be used for the encapsulation of organic electronic devices.[4–8]

ZnO nanoparticles impregnated onto the PVA matrix can significantly modify/alter the electrical, optical and mechanical properties.[9–11] Also, these composites show unusual charge conduction behaviour.[12] It has been shown that polyvinyl alcohol/clay nanocomposites can be used for the encapsulation of organic solar cells.[13] PVA films also exhibit excellent oxygen barrier properties (at low relative humidity)[14] and are also a potential material for solar cell encapsulation.[15] Due to low O_2 permeability of polyvinyl alcohol, photo-oxidation can only occur up to 5 μm within the exposed surface.

*[a]Department of Materials Engineering, Bangalore, India.
E-mail: praveen@materials.iisc.ernet.in; Fax: +91-80-2360-0472;
Tel: +91-80-2293-2627*
*[b]Center for Nanoscience and Engineering, Indian Institute of Science,
Bangalore, India. E-mail: praveen@materials.iisc.ernet.in;
Fax: +91-80-2360-0472; Tel: +91-80-2293-2627*
† Electronic Supplementary Information (ESI) available: See DOI:
10.1039/c2ra21714g

Semiconductor (like TiO_2, ZnO) based photo-catalysts are used to enhance the rate of photo reactions under milder conditions. This involves the generation of holes (h^+_{VB}) and electrons (e^-_{CB}) by the band gap excitation of a semiconductor photo-catalyst surface, when it is exposed to UV or visible light ($h\nu \geqslant E_{Band}$). These charge carriers, when reacted with water and oxygen, produce reactive hydroxyl and superoxide radicals, which mediate oxidation and reduction reactions. Thus, the photoactive ZnO nanoparticles can trap oxygen and moisture at the surface and when these molecules permeate through the matrix. Barrer *et al.*[16] have observed that micron-sized ZnO particles can reduce the permeability of gases in natural rubber.

Even though the conventional techniques like ALD/MLD and multilayered routes for encapsulation have several advantages, these processes are complex and suffer from poor scalability. Inorganic oxide based thin films (Al_2O_3, SiO_x) exhibit good barrier properties, but the generation of pin holes and cleavages creates problems for their use as barrier materials. Bare flexible plastic substrates with polyolefins like polypropylene and polyethylene show a water vapor transmission rate (WVTR) in the range 1–6 g m^{-2} day^{-1} and an oxygen transmission rate (OTR) of 70–600 cm^3 m^{-2} day^{-1} and thus do not meet the requirement of a barrier material demanding ultra-low barrier permeability.

The present work discusses the fabrication of reactive barrier films based on polyvinyl alcohol as the base polymer matrix impregnated with zinc oxide nanoparticles. The dispersed inorganic phase was anticipated to provide a tortuous pathway for the incoming gas molecules, retarding the intrusion, thereby reducing permeability through the matrix. Therefore, hybrid polymer nanocomposites processed by a simple technique, that can serve as a moisture/oxygen barrier material, would be a better option than those processed by conventional techniques,

but still further improvement is required in terms of the barrier property.

Materials

Polyvinyl alcohol (M_w = 86, 00, 000) was purchased from S. D Fine Chem (India). The zinc oxide (ZnO) nano powder (average particle size 80–100 nm, specific surface area 10–25 m^2 g^{-1}) was obtained from Alfa Aesar (USA). Triethanoltriamine was obtained from Ranbaxy (India). Millipore water was used for the preparation of composites.

Composite preparation

The composites were fabricated by following a simple solution casting methodology, using water as a solvent. PVA polymer (in powder form) was dissolved in deionized water by maintaining a ratio of 30 ml g^{-1} and stirring at 50 °C for 2 h. Various wt% (0.5, 1.0, 2.0 and 4.0) of ZnO nanoparticles (previously dried at 110 °C in vacuum oven) were added and sonicated for 0.5 h. This was followed by the addition of TEOA (triethylenetriamine) to the dispersion (in a weight ratio of 5 wt% with respect to the polymer) and it was stirred for 48 h. The homogeneous solution was then transferred to a Teflon coated mould and dried at ambient pressure for 6 days and under vacuum at 40 °C to obtain the dry composite films. A control polymer film (PVA) was prepared by following the same procedure without the nano-particles. The flexible freestanding films were then taken out from the cast (average thickness ~250 μm) and further analyses were carried out. The pristine polymers, with 0.5 wt%, 1.0 wt% and 2.0 wt% and 4.0 wt% loadings of zinc oxide nanoparticles are designated as PV0, PV0.5, PV1, PV2 and PV4, respectively.

Characterizations

The FTIR (Fourier transformed infrared) spectroscopy of the ZnO nanopowder was carried out in a Thermo Nicolet 6700 instrument in the range 400 to 4000 cm^{-1}, with a spectral resolution of 4 cm^{-1}. The spectra were recorded using the potassium bromide (KBr) pellet method. The solid state diffuse reflectance UV-visible spectrum of the neat ZnO nanopowder was monitored using a Perkin Elmer (Model-Lambda 35) instrument and the phase analysis was carried out in an X'pert pro instrument. UV-visible analysis of the composites and the polymer films was also carried out in a Perkin Elmer (Model-Lambda 35) instrument in a wavelength range 190 to 1100 nm. For this analysis, free standing films of PV0, PV1 etc. of 250 μm were cut into discs of 0.5 cm and placed in the sample holder.

Thermal phase transition of the neat polymer and ZnO filled nanocomposites were studied using a Mettler Toledo (DSC 822^e) instrument at a heating rate of 10 °C min^{-1} in an argon atmosphere with a flow rate of 80 ml min^{-1} in a hermetically closed aluminum pan. The DSC instrument was calibrated using standard indium and zinc specimens prior to the experiment.

The thermal stability of the neat polymer and nanocomposite films was investigated by measuring the loss in mass as a function of temperature using a high-resolution TGA 2950 (NETZSCH - STA 409PC) in an argon atmosphere at a heating rate of 10 °C min^{-1}. For thermo mechanical property analysis, DMA (dynamic mechanical analysis) of the composites was carried out in MetraVib DMA$^+$100, in tensile mode applying a constant frequency of 1 Hz, in the temperature range 30 °C to 100 °C. A static force of 0.5 N and dynamic force of 2 N was applied to the samples. The static contact angle measurement of the PVA composite films was carried out in ambient conditions, in an OCA 30 goniometer (Dataphysics, Germany) that contains a stepper motor to control the volume (3 μL) of the liquid (millipore water) supplied from a microsyringe. For each sample, at least five readings were taken at different positions. In case of the SEM analysis of neat ZnO, the powder specimen was coated over carbon tape, sputter coated with gold, and high resolution FESEM (Carl Zeiss) was used to observe the morphology (at 26.7 KX and 53.86 KX magnifications). The SEM analysis of the composites were carried out in an ESEM-Quanta. Cryogenically fractured surfaces of the composites and the neat polymer samples were used for the SEM analysis; they were sputter coated with gold, prior to SEM analysis. Optical microscopic images of the composites were observed in transmittance mode using an Axiovert 200 MAT inverted microscope.

A density gradient column was used in order to measure the specific gravity of the composites by following ASTM D1505 as a standard. The column was prepared by using tetrahydrofuran (d = 0.816 g cc^{-1}) and carbon tetrachloride (d = 1.59 g cc^{-1}), which consists of a cylindrical glass 1 m long containing the solution of tetrahydrofuran (THF) and carbon tetrachloride (CCl_4), having a linear gradient of density from the top (lower density) side to the bottom (higher density) side of the column. The mixtures of THF/CCl_4 (v/v): 100 : 0, 90 : 10, 80 : 20, 70 : 30, 60 : 40, 50 : 50, 40 : 60, 30 : 70, 20 : 80, 10 : 90 and 0 : 100 were prepared and slowly poured down the sides of the tube in order to avoid any mixing of the layers. Standard calibrated density markers in the form of glass beads (H & D Fitzgerald Ltd., St. Asaph, UK), along with the composites, were dropped into the column. The specific gravity of the composites was calculated by comparing the position of the composites with that of the standards.

Permeability measurement of the composites: calcium degradation test

The water vapor transmission rates and the permeability behavior of the composite films were determined using the calcium degradation test. This follows a previously discussed method,[17] wherein 1 cm × 1 cm of calcium, having a thickness of 150 nm and aluminium of 200 nm thickness on either side of calcium (to provide electrical connectivity for resistance mea-surement) were deposited separately over a thoroughly cleaned glass slide using various shadow masks. This was carried out inside a Mbraun glove box (ultra high pure Argon atmosphere), connected to a thermal evaporator. The glass slide, when sealed, acts as a moisture sensor, as calcium reacts with moisture increasing the resistance accordingly. The glass substrate deposited with calcium and aluminium was covered with the composite film so that the calcium deposited area was totally enclosed by the film. The edges were sealed with glue that cures at room temperature (Epoxy Lapox L12) to minimize the leakage through the gap between the film and calcium deposited glass slide. In order to verify the water vapor leakage rate through the glue, a control experiment was carried out by sealing

a glass substrate with the same glue. These sealed glass slides were kept inside a programmable humidity chamber (RH = 90% and T = 25 °C, Kaleidoscope, India, Model Number-KEW/PHC-80) and the variation of resistance with time was measured.

Accelerated weathering studies of encapsulated devices

Schottky structured organic devices were fabricated and encapsulated with the as-prepared composite films to study their applications as a barrier material. About 1 wt% poly (3-hexylthiophene) (P3HT) was dissolved in chlorobenzene. P3HT was synthesized by a previously reported method.[18] The ITO coated glass slides of dimensions 25.4 mm × 25.4 mm were pretreated to etch out the ITO coatings from the sides, so that the effective ITO area becomes 25.4 mm × 15 mm. Then the solution of P3HT in chlorobenzene (about 150 μL) was spincoated at a speed of 1000 RPM for 10 s onto a cleaned ITO coated glass slide. This was then annealed at 130 °C for 10 min. Then aluminium (contact area of 4 mm^2) was deposited over the P3HT layer using a shadow mask by thermal evaporation. These devices were encapsulated with the composite films, using the same glue that was used in the calcium degradation test for sealing the edges. The I–V characteristics of the fabricated devices were measured using a source meter (Keithley, Model 2420). The devices were subjected to accelerated ageing by placing them in a humidity chamber, maintained at a RH of 90% at 25 °C.

Results and discussion

Fabrication of the composite films

PVA/ZnO composite films were prepared by following a solution casting method. In the composite fabrication, the ZnO nanoparticles in a desired ratio were dispersed in a polymer/solvent (using water as a solvent) system. The ZnO nanoparticles were used as an inorganic phase for the polymer matrix and were supposed to provide a tortuous pathway for gas molecules like oxygen and moisture, penetrating through the matrix. An additional phase of triethanolamine was also used for the composite matrix. It was expected to serve two purposes: one is to provide more polar groups in the matrix and the second is to act as a sacrificial electron donor.[19] Hence, it can react with H_2O and O_2 trapped at the surface under UV irradiation.

Pristine zinc oxide (ZnO) nanoparticle characterizations

The FTIR spectrum of pure ZnO shows a peak at around 558 cm^{-1}, which is due to the Zn–O vibration, and a broad peak around 3430 cm^{-1} corresponds to the stretching of –OH groups at the surface of ZnO nanoparticles (Fig. 1A). The peak around at 2260 cm^{-1} is due to adsorbed CO_2 at the surface (Fig. 1). XRD peaks correspond to the wurzite phase of the as-used ZnO sample (Fig. 1B). The SEM images show the aggregated image of ZnO nanopowder (Fig. 1C). UV-visible spectra show an absorption edge of 375 nm corresponding to a band gap of $\sim$3.29 eV (Fig. 1D).

Composite studies

Thermal characterizations

It is important for a barrier material to protect the device active components from odd/high thermal environments. From the

TGA thermogram (Fig. 2), it is observed that the composites showed a reduced degradation temperature, as compared to the PV0. It can also be observed that the onset of degradation for all the composites is $\sim$252 °C. However, the composites show an improvement in the degradation temperature at 60% and 70% of degradation. The 60% degradation temperature ($T_{d\ 60\%}$) for PV1 was 319 °C, which improved to 374 °C for PV4, and the 70% degradation temperature ($T_{d\ 70\%}$) for PV1 was 385 °C, while it was 410 °C for PV4. DSC analysis of the polymer (PV0) and the composite (Fig. 3) in the specific temperature range showed that the melting peak appeared at a temperature of 157 °C. The peak position was observed to be nearly independent (± 2 °C) of the ZnO loadings.

Mechanical behavior of the composites

An increase in the T_g was observed (Fig. 4A) from PV0.5 (55 °C) to PV2 (60 °C), as observed from the plot of tan δ as a function of temperature. The T_g of PV4 ($\sim$59 °C) is similar to PV2, possibly due to the aggregation effect exhibited by ZnO nanoparticles, as also observed from AFM images (discussed later). Interestingly, DSC analysis of the polymer as well as the films did not show any glass transition peak. The relative changes in storage modulus (E') as a function of temperature for the composites indicate a steady increase in the modulus value (Fig. 4B). However, PV4 showed a relative reduction in the modulus, which could be due to the effect of aggregation of ZnO nanoparticles in the matrix.

FTIR spectra, fractured surface SEM and the density measurement of the composites

The FTIR spectra of ZnO, PV0, PV0.5 and PV2 are shown in Fig. S1 (ESI †). PV0.5 and PV2 showed a peak around 558 cm^{-1}, which is due to the incorporation of ZnO in the matrix and was not observed for PV0. The other peaks (2940 cm^{-1}, –CH$_2$ asymmetric stretching vibration; 2840 cm^{-1}, –CH$_2$ symmetric stretching vibration; 1431 cm^{-1}, –C–C stretching) indicate the basic PVA structural backbone. The cross-section of cryogenically fractured surfaces of the composites shows more cracks/breakages, indicating a better interfacial interaction between the polymer matrix and the nanoparticles after nanocomposite formation (Fig. S2, ESI †), as compared to PV0.

For neat polymer films, a density of 1.185 g cc^{-1} was observed while the value increased to 1.235 g cc^{-1} for PV4 (Fig. 5). The density plot, with respect to the position of the standard reference beads in the same solvent mixture, is shown in Fig. S3 (ESI †). The increase in density of the composite is due to the increase in ZnO loadings and better integration of the ZnO nanoparticles in the matrix.

Optical property of the composites

UV-visible spectra of the composites show a reduction in the percentage transmittance with an increase in ZnO loading (%)[20] (Fig. 6A), which indicates that composite transparency to light is affected by the presence of the ZnO particles. This is due to the increased ZnO concentration in the composite matrix. The figure also shows that the composite matrix
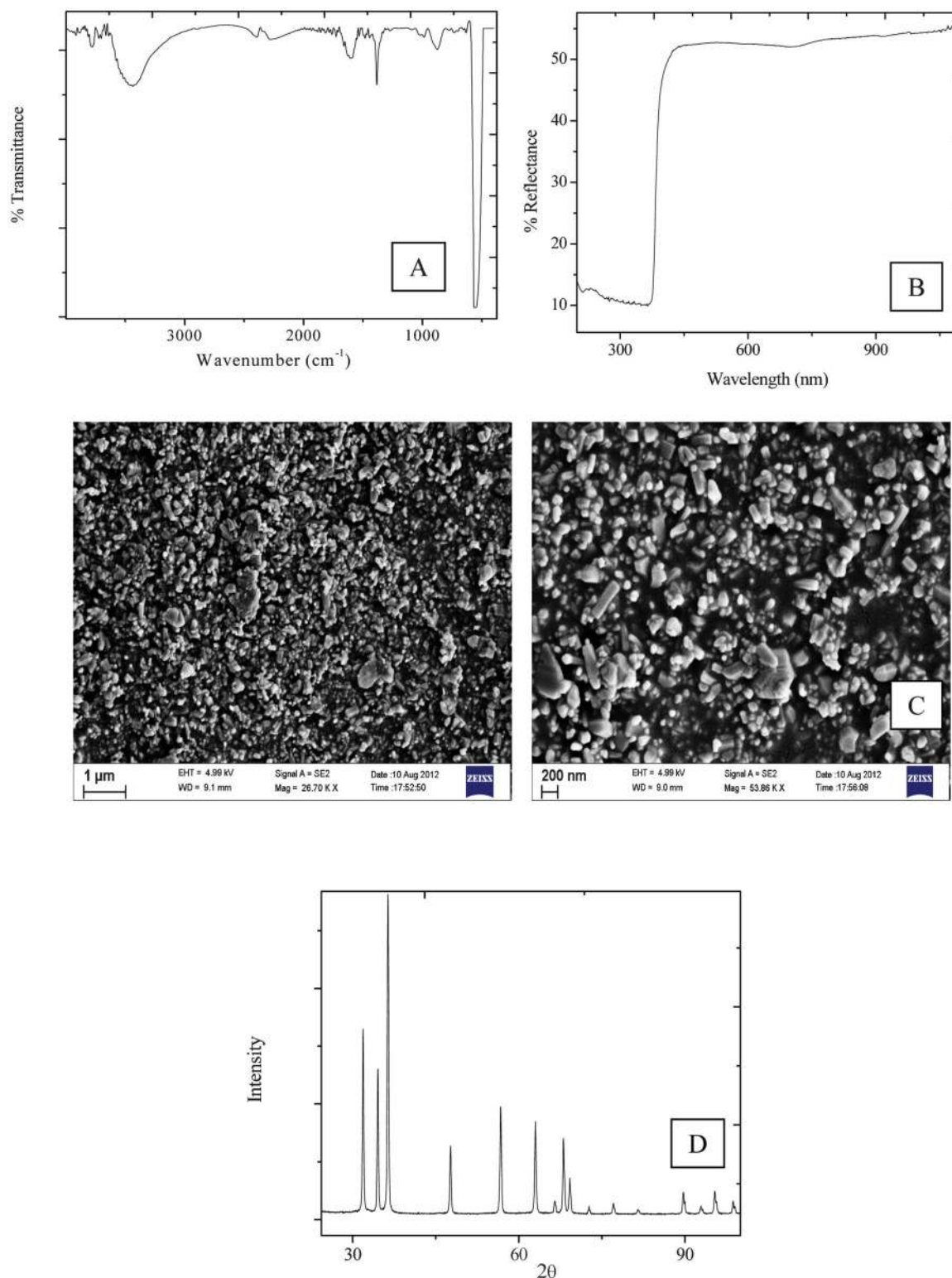
Fig. 1 (A) FTIR spectra (B) UV-vis spectra (C) SEM of pristine ZnO (D) XRD spectra of pristine ZnO.

absorbs in the UV region, due to the presence of semiconducting ZnO nanoparticles. The percentage transmittance at 700 nm is also plotted in the inset of (Fig. 6B), which shows the trend in the reduction.

Surface characteristics and the surface morphology of the composites

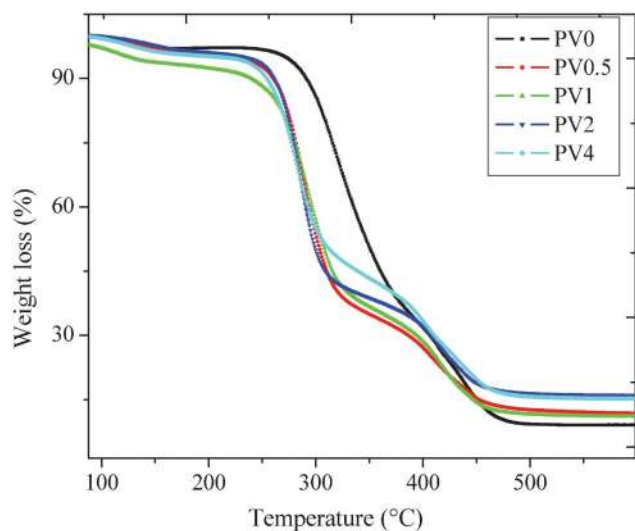Contact angle measurement values for the polymer and the nanocomposites show a reduction in the value (PV0: $70 \pm 2°$,

Fig. 2 Thermogravimetric analysis of the composites.

PV2: $63 \pm 0.5°$, PV4: $59 \pm 1°$). The reduction in contact angle (*i.e.* the increase in wettability) with respect to the neat polymer is due to the increase in hydrophilic ZnO particles, as well as due to the addition of the polar TEOA in the matrix, which will increase the hydrophilic character as well. A similar reduction in contact angle with the increase in hydrophilic particle loading in composite films was also observed in a previous study.[13]

The AFM images indicate (Fig. 7) an increase in the surface inhomogeneity. The optical microscopy images (Fig. S4, ESI †) of the films also showed that the non-uniform film surfaces may be due to the increase in the ZnO content in the matrix, leading to agglomeration in the matrix. With the increase in particle loading, a similar type of agglomeration behavior was also observed in previous studies.[5,20] The agglomeration effect is also observed in the AFM image of PV4. This can also enhance the wettability of the matrix.[13] The result of this aggregation has also been reflected in the mechanical properties, which showed a reduction in the storage modulus.
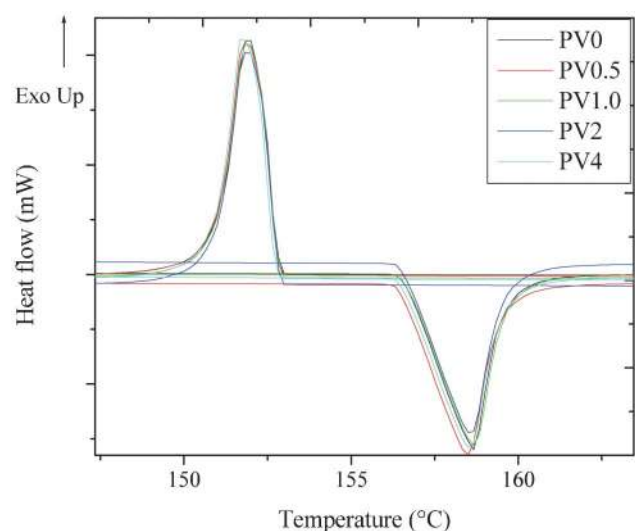
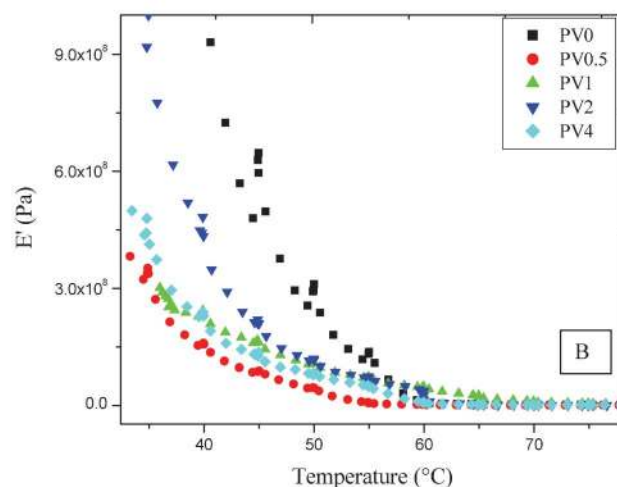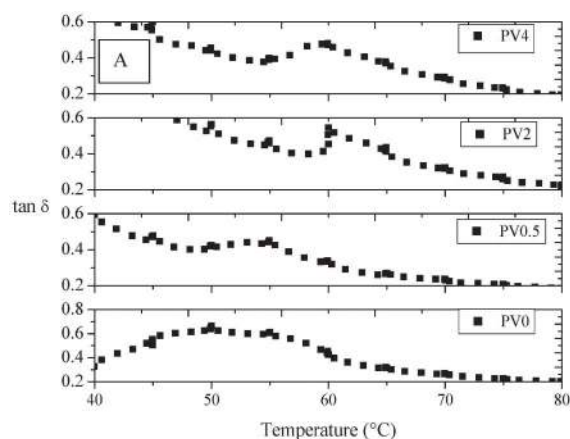**Fig. 4** DMA analysis of the composites (A) tan δ *vs.* temperature and (B) storage modulus *vs.* temperature.

Fig. 3 DSC analysis of the composites.
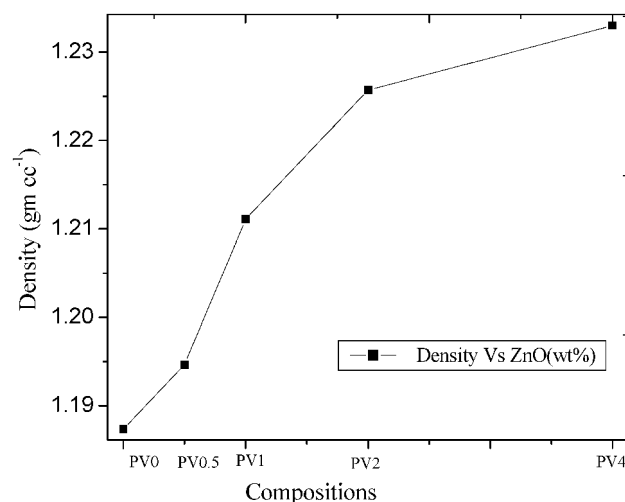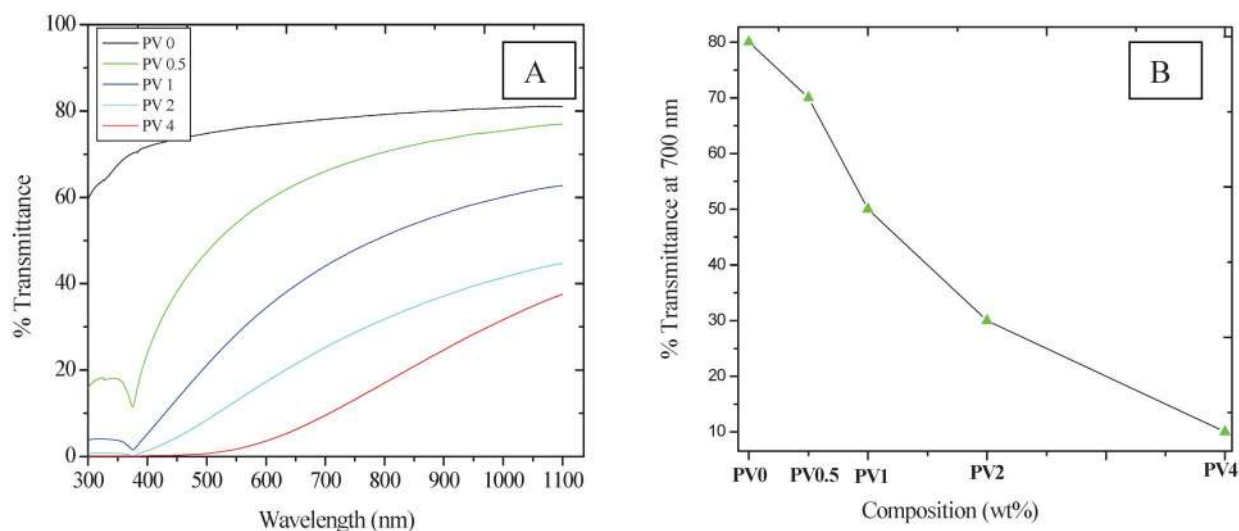

Fig. 5 Density analysis of the composites.

Fig. 6 Optical properties of the composites.

Permeability measurement of the composites

The variation of the inverse of normalized resistance (R_0/R) with time for the neat polymer film, both the composites and neat glue at 90% RH and $T = 25 \pm 0.2$ °C are shown in Fig. 8. Water vapor transmission rates have been calculated at each time by determining the derivative at all points for the R_0/R vs. time plot and are shown in Fig. 9. The average transmission rates for different time intervals for the three compositions are given in Table 1. Table 1 shows the thermally deposited calcium layer completely degraded after 3300 s for PV4, 200 s for PV1 and 90 s for PV0. This indicates that the presence of ZnO in the matrix improves the barrier property of the composite. The average permeability value gradually decreases from PV0 to PV1 to PV4. This relative reduction in the WVTR of the composites shows

the improved barrier property with increase in ZnO loading, which can be attributed to the decreased permeation rate of moisture molecules through the matrix by the incorporation of ZnO nanoparticles.

Determination of water vapor diffusivity from calcium degradation test

The diffusion coefficients (D) for water vapor permeation through the neat polymer and the composites were determined using Fick's laws of diffusion for a one dimensional membrane. The cumulative amount of water vapor (Q) transmitted through the membrane of thickness l at time t, assuming the concentration of water vapor to be zero on one side of the membrane, is given by[21,22]
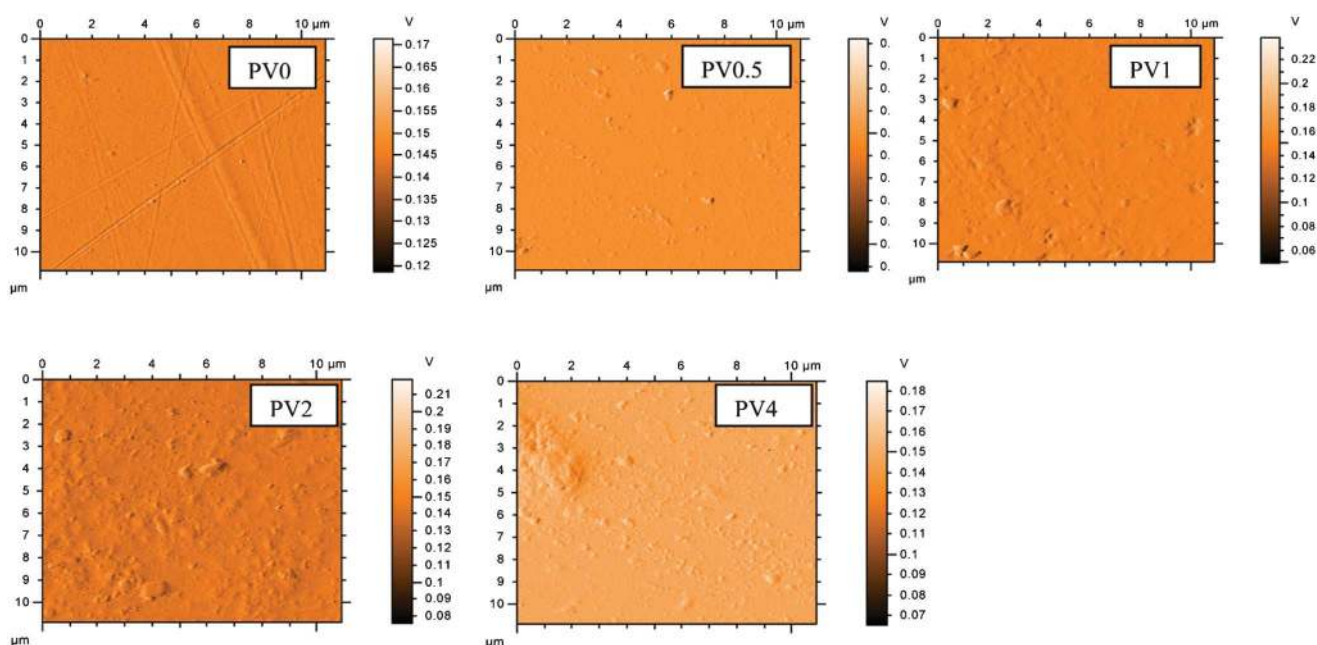

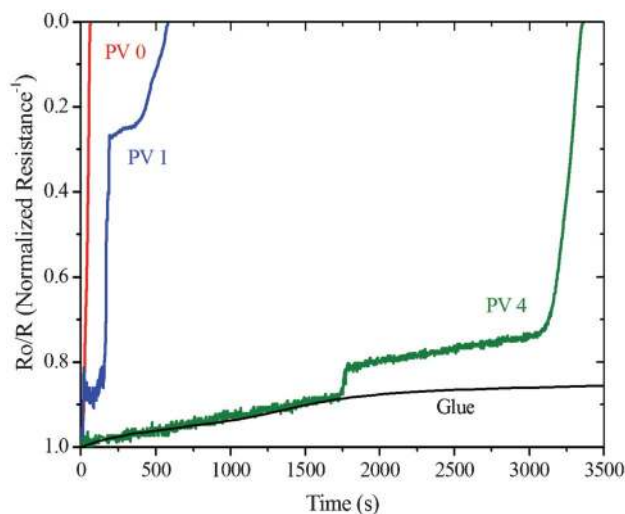**Fig. 7** AFM images of the composites.

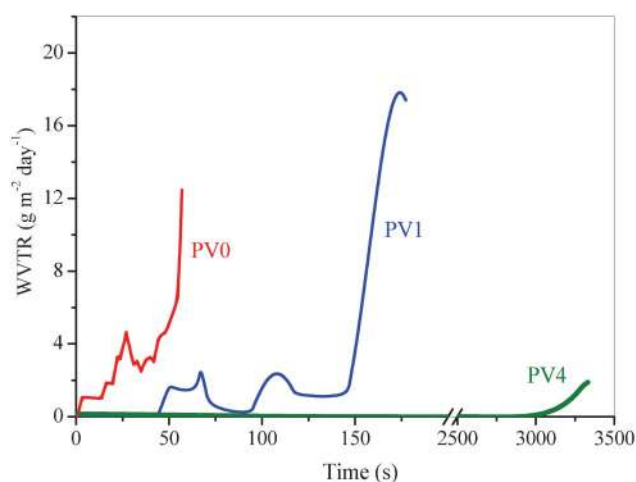**Fig. 8** Normalized conductance *vs.* time plot for PV0, PV1 and PV4.

Fig. 9 Permeability value obtained from the slope of each point.

$$\frac{Q}{lc} = \frac{Dt}{l^2} - \frac{1}{6} - \frac{2}{\pi^2} \sum_{n=1}^{\infty} \frac{(-1)^n}{n^2} \exp\left(-\frac{Dn^2\pi^2 t}{l^2}\right) \qquad (1)$$

The concentration, c, corresponds to 90% humidity at 25 °C (equivalent to 20.71 g m^{-3}) on the other side of the membrane.

From the calcium degradation test, the cumulative amount of water vapor (Q) transmitted at any time t, can be experimentally determined from

$$Q = (\Delta\frac{1}{R})\rho\delta(\frac{L}{B}) \qquad (2)$$
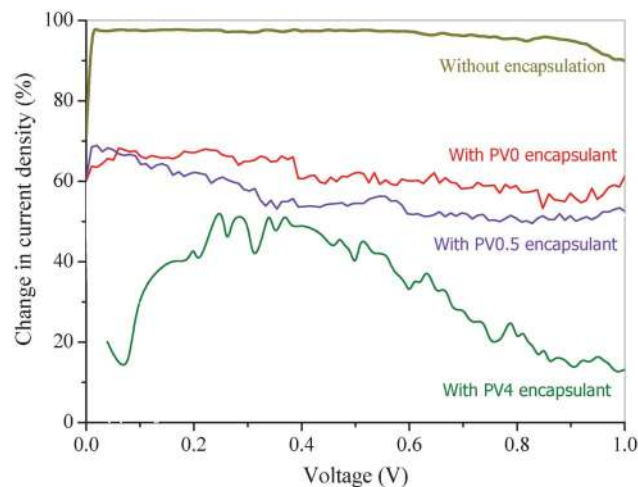

Fig. 10 Diode characteristic of the devices with and without encapsulation after 0.5 h at 90% RH at 25 °C.

where R is resistance, ρ is density of calcium, δ is resistivity of calcium, and L and B are the length and width of the deposited calcium.

Eqn (1) was solved non-linearly using the experimentally determined Q, t and l to evaluate the diffusion coefficient D. This value corresponds to 7.01×10^{-10} m^2 s^{-1}, 5.37×10^{-10} m^2 s^{-1} and 9.17×10^{-12} m^2 s^{-1} for PV0, PV1 and PV4, respectively. This value is higher than that observed for liquid water (2.16×10^{-11} m^2 s^{-1} through PVA of M_w 90 000 at 20 °C) but lower than that for oxygen (1.8×10^{-9} m^2 s^{-1} at 25 °C) as well as argon (1.2×10^{-9} m^2 s^{-1}). The significantly lower value of D for PV4 compared to PV0 indicates that the nanocomposite reduces the permeability.

Device characteristics under accelerated weathering

The I–V characteristics of the encapsulated (with PV0, PV0.5 and PV4) and non-encapsulated Schottky structured devices, before (to get initial I–V characteristics) and after ageing (exposing to 90% RH at 25 °C for 0.5 h) were measured using a source-meter (Keithley, 2420). Therefore, after 0.5 h ageing, the reduction in current densities with respect to the initial device characteristics was determined over a voltage range 0 to 1 V. The percentage change [$100 \times (I_0 - I)/I_0$, where I_0 is initial current density] in current density (I) for each device was calculated with respect to the initial current density over the 0 to 1 voltage range, as shown in Fig. 10. The current density decreased with time under humidified air/oxygen for all the devices but the decrease was highest for the unencapsulated device and lowest for the PV4 encapsulated device. It can be observed (Fig. 10) that after 0.5 h the relative reduction in current density is 30 ± 7% for the PV4,

Table 1 Average WVTR for the composites at various time intervals

Average WVTR (g m^{-2} day^{-1})							
Composite	90 s	90–150 s	150–200 s	200–1500 s	1500–3000 s	3000–3300 s	
PV0	4.200	end	—	—	—	—	—
PV1	0.6340	1.4535	13.0483	end	—	—	—
PV4	0.0951	0.0240	0.0088	0.0229	0.0426	0.7617	end

55 ± 5% for the PV0.5, 67 ± 5% for PV0 and 97 ± 1% for the non-encapsulated device within the voltage range 0 to 1 V. The relative decrease in percent change of current density from PV0 to PV4 after 0.5 h ageing is due to the decrease in moisture permeation rate with increase in ZnO loading. Moreover, the non-encapsulated device completely fails after 0.5 h ageing. However, the devices encapsulated with the composites were comparatively stable up to 2 h. Also, the composites showed insignificant swelling after a prolonged exposure to high relative humidity (90%).

Conclusions

Solution cast PVA films impregnated with ZnO nanoparticles were prepared for device encapsulation. The primary results indicate that an optimum concentration is required for the application, as increased loading results in agglomeration in the matrix. Even though the thermal properties deteriorate for the composites, as compared with PV0, a reduction in the permeability was observed with the incorporation of ZnO nanoparticles in the matrix. Further studies on the permeability behavior of the composites under UV/solar radiation are required to further demonstrate the reactive composites as a barrier material. Encapsulation of devices shows that higher loading of ZnO is better for encapsulation. This kind of reactive barrier material can be sandwiched between two non reactive (polyvinylbutyral (PVB), cyclic olefin copolymer (COC) polymer layers to get an efficient sandwiched material, which can be used for the encapsulation of organic devices.

Acknowledgements

References

1 R. B. Ye, M. BaBa, K. Suzuki, Y. Ohishi and K. Mori, *Thin Solid Films*, 2004, **464–465**, 437–440.
2 R. D. Scurlock, B. Wang, P. R. Ogilby, J. R. Sheats and R. L. Clough, *J. Am. Chem. Soc.*, 1995, **117**, 10194–10202.
3 D. G. J. Sutherland, J. A. Carlisle, P. Elliker, G. Fox, T. W. Hagler, I. Jimenez, H. W. Lee, K. Pakbaz, L. J. Terminello, S. C. Williams, F. J. Himpsel, D. K. Shuh, W. M. Tong, J. J. Lia, T. A. Callcott and D. L. Ederer, *Appl. Phys. Lett.*, 1996, **68**, 2046–2048.
4 S. Gupta, P. C. Ramamurthy and G. Madras, *Ind. Eng. Chem. Res.*, 2011, **50**, 6585–6593.
5 S. Gupta, P. C. Ramamurthy and G. Madras, *Polym. Chem.*, 2011, **2**, 221–228.
6 S. Gupta, P. C. Ramamurthy and G. Madras, *Thermochim. Acta*, 2011, **524**, 74–79.
7 S. Gupta, P. C. Ramamurthy and G. Madras, *Polym. Chem.*, 2011, **2**, 2643–2650.
8 J. S. Lin, M. H. Chung, C. M. Chen, F. S. Juang and L. C. Liu, *J. Phys. Org. Chem.*, 2011, **24**, 193–202.
9 V. Senthil, T. Badapanda, S. N. Kumar, P. Kumar and S. Panigrahi, *J. Polym. Res.*, 2012, **19**, 9838.
10 M. Hema, S. Selvasekerapandian and G. Hirankumar, *Ionics*, 2007, **13**, 483–487.
11 M. B. Muradov, A. Sh. Abdinov, R. H. Hajimamedov and G. M. Eyivazova, *Surface Engineering and Applied Electrochemistry*, 2009, **45**, 167–170.
12 G. Chakraborty, K. Gupta, A. K. Meikap, R. Babu and W. J. Blau, *J. Appl. Phys.*, 2011, **109**, 033707.
13 J. Gaume, C. Taviot-Gueho, S. Cros, A. Rivaton, S. Therias and J. L. Gardette, *Sol. Energy Mater. Sol. Cells*, 2012, **99**, 240–249.
14 J. H. Yeun, G. S. Bang, B. J. Park, S. K. Ham and J. H. Chang, *J. Appl. Polym. Sci.*, 2006, **101**, 591–596.
15 J. Gaume, P. Wong-Wah-Chung, A. Rivaton, S. Therias and J. L. Gardette, *RSC Adv.*, 2011, **1**, 1471–1481.
16 R. M. Barrer, J. A. Barrie and M. G. Rogers, *J. Polym. Sci., Part A: Polym. Chem.*, 1963, **1**, 2565–2586.
17 R. Paetzolda, A. Winnacker, D. Henseler, V. Cesari and K. Heuser, *Rev. Sci. Instrum.*, 2003, **74**, 5147–5150.
18 R. D. McCullough, *Adv. Mater.*, 1998, **10**, 93–116.
19 A. M. Peiro, G. Doyle, A. Mills and J. R. Durrani, *Adv. Mater.*, 2005, **17**, 2365–2368.
20 J. Lee, D. Bhattacharyya, A. J. Easteal and J. B. Metson, *Curr. Appl. Phys.*, 2008, **8**, 42–47.
21 J. Crank, *The Mathematics of Diffusion*, Oxford University Press, Oxford, UK, 2nd edn, 1975, ch. 4, pp. 44–68.
22 S. Schubert, H. Klumbies, L. Müller-Meskamp and K. Leo, *Rev. Sci. Instrum.*, 2011, **82**, 094101–094108.